STEM CELLS TRANSLATIONAL MEDICINE®

EMBRYONIC STEM CELLS/INDUCED PLURIPOTENT STEM (iPS) CELLS

Small Molecule-Mediated Directed Differentiation of Human Embryonic Stem Cells Toward Ventricular Cardiomyocytes

IOANNIS KARAKIKES,[a,*] GRANT D. SENYEI,[a,*] JENS HANSEN,[b] CHI-WING KONG,[c] EVREN U. AZELOGLU,[b] FRANCESCA STILLITANO,[a] DEBORAH K. LIEU,[c] JIAXIAN WANG,[c] LIHUAN REN,[c] JEAN-SEBASTIEN HULOT,[a] RAVI IYENGAR,[b] RONALD A. LI,[a,c] ROGER J. HAJJAR[a]

Key Words. Cardiac • Embryonic stem cells • Pluripotent stem cells • Differentiation

[a]Cardiovascular Research Center and [b]Department of Pharmacology and Systems Therapeutics, Systems Biology Center, Icahn School of Medicine at Mount Sinai, New York, New York, USA; [c]Stem Cell and Regenerative Medicine Consortium, Department of Physiology, LKS Faculty of Medicine, University of Hong Kong, Hong Kong

[*]Contributed equally as first authors.

Correspondence: Ioannis Karakikes, Ph.D., Stanford University School of Medicine, Stanford Cardiovascular Institute, 300 Campus Drive, Grant S114, Stanford, California 94305, USA. Telephone: 650-736-2863; Fax: 650-736-0234; E-Mail: ioannis.karakikes@stanford.edu

Received June 7, 2013; accepted for publication August 20, 2013.

1066-5099/2013/$20.00/0

http://dx.doi.org/10.5966/sctm.2013-0110

ABSTRACT

The generation of human ventricular cardiomyocytes from human embryonic stem cells and/or induced pluripotent stem cells could fulfill the demand for therapeutic applications and in vitro pharmacological research; however, the production of a homogeneous population of ventricular cardiomyocytes remains a major limitation. By combining small molecules and growth factors, we developed a fully chemically defined, directed differentiation system to generate ventricular-like cardiomyocytes (VCMs) from human embryonic stem cells and induced pluripotent stem cells with high efficiency and reproducibility. Molecular characterization revealed that the differentiation recapitulated the developmental steps of cardiovascular fate specification. Electrophysiological analyses further illustrated the generation of a highly enriched population of VCMs. These chemically induced VCMs exhibited the expected cardiac electrophysiological and calcium handling properties as well as the appropriate chronotropic responses to cardioactive compounds. In addition, using an integrated computational and experimental systems biology approach, we demonstrated that the modulation of the canonical Wnt pathway by the small molecule IWR-1 plays a key role in cardiomyocyte subtype specification. In summary, we developed a reproducible and efficient experimental platform that facilitates a chemical genetics-based interrogation of signaling pathways during cardiogenesis that bypasses the limitations of genetic approaches and provides a valuable source of ventricular cardiomyocytes for pharmacological screenings as well as cell replacement therapies. STEM CELLS TRANSLATIONAL MEDICINE *2014;3:1–14*

INTRODUCTION

The adult heart has a limited intrinsic capacity to regenerate lost or damaged myocardium, with ventricular cardiomyocyte deficiency underlying most causes of heart failure. Cardiomyocytes derived from human embryonic stem cells (hESCs) are a potential source for cell replacement therapy and an invaluable tool in the investigation of cardiac development, disease modeling, and drug testing, but despite considerable progress, increasing the efficiency of differentiating hESCs toward ventricular cardiomyocytes has been very challenging.

The myocardium is composed of multiple highly specialized myocardial lineages, including those of the ventricular and atrial myocardium and the specialized conduction system [1]. An evolutionarily conserved gene regulatory network of transcription factors orchestrates the specification and maturation of each of these lineages during heart development, which is controlled by a plethora of extracellular instructive, spatiotemporally regulated signaling molecules [2]. Among these molecules are fibroblast growth factors, Wnt proteins, members of the transforming growth factor β superfamily, bone morphogenic proteins (BMPs), activin, and nodal [3]. Similarly, exposing hESCs to a combination of signaling molecules that mimic the developmental cues can induce cardiogenesis in vitro; however, the generation of a homogeneous population of cardiomyocytes remains an important limitation of the current methodologies. The existing cardiomyocyte-differentiation protocols generate a heterogeneous cell population consisting of atrial-, nodal-, and ventricular-like cardiomyocytes (VCMs) with variable yields [4–10]. The isolation of pure populations of VCMs requires viral vector-mediated genetic manipulation to enable either drug selection or cell sorting [11–13], which precludes their use in downstream cell-based therapies. In addition, batch-to-batch inconsistencies of serum and the high cost of multiple growth factors used in conventional differentiation protocols are major limitations for large-scale production.

Chemical biology approaches using readily available and inexpensive synthetic bioactive

molecules that regulate stem cell fate could potentially rectify these problems [14]. Small molecules that can control cellular processes by modulating signal transduction pathways have been used effectively in hESC differentiation protocols, including cardiomyocytes [15–17], neural progenitors [18], and endodermal linages [19].

In this paper, we describe the development of a fully chemically defined, small molecule-mediated directed differentiation protocol that drives differentiation of hESCs toward VCMs. The protocol is efficient, reproducible, and cost effective, producing a nearly pure population of VCMs without genetic manipulation or cell sorting. Our cardiomyocyte-differentiation protocol represents a reproducible and efficient model system to investigate biologically relevant mechanisms that govern cardiovascular lineage commitment and provides a renewable source of VCMs for pharmacological screenings and cell replacement therapies.

Materials and Methods

Cell Culture and Cardiomyocyte Differentiation

The human embryonic stem cell lines HES-2 (ES02), H7 (WA07), and H1 (WA01) were obtained from the WiCell Research Institute (Madison, WI, http://www.wicell.org). The induced pluripotent stem cell (iPSC) line (SKiPS-33.1) was derived by the reprogramming of human dermal fibroblast obtained from a skin biopsy of a 45-year-old volunteer with informed consent (Staten Island University Hospital, Staten Island, NY), as described [20]. All lines were propagated under feeder-independent conditions, as described [21]. Briefly, the hESCs and iPSCs were maintained in the mTeSR1 median (StemCell Technologies, Vancouver, BC, Canada, http://www.stemcell.com) on hESC-qualified Matrigel-coated dishes (BD Biosciences, San Diego, CA, http://www.bdbiosciences.com) in 5% carbon dioxide, 5% oxygen, and 90% nitrogen environment at 37°C.

The cells were induced to differentiate by culturing in mTeSR1 medium supplemented with BMP4 (10 ng/ml^{-1}) and blebbistatin (5 μM) in suspension on ultra-low-attachment dishes (Corning Life Sciences, Acton, MA, http://www.corning.com/lifesciences) for one day (day 0–1). The next day, the medium was switched to basal differentiation medium (StemPro 34, 50 μg ml^{-1} ascorbic acid, 2 mM GlutaMAX-I; Life Technologies, Rockville, MD, http://www.lifetech.com) supplemented with BMP4 (10 ng/ml^{-1}) and activin A (25 ng/ml^{-1}) and maintained for 48 hours (days 1–3). Then the medium was switched to basal differentiation medium for another 36 hours (days 3–4.5). Finally, the cells were differentiated in basal differentiation medium supplemented with IWR-1 (2.5 μM) for 96 hours (days 4.5–8.5) (protocol is summarized in supplemental online Table 1). The differentiated cardiomyocytes were maintained in basal differentiation media for up to 4 weeks. All cytokines were purchased from R&D Systems Inc. (Minneapolis, MN, http://www.rndsystems.com). The small molecules were purchased from Sigma-Aldrich (St. Louis, MO, http://www.sigmaaldrich.com). All differentiation cultures were maintained in 5% carbon dioxide air environment.

Flow Cytometry and Immunocytochemistry

Single-cell suspensions were obtained by dissociating differentiation cultures with (0.04% trypsin, 0.03% ethylenediaminetetraacetic acid) for 15 minutes at 37°C. The cells were then fixed (3.6% paraformaldehyde) for 15 minutes and washed twice with phosphate buffered saline (PBS). The fixed cells were first permeabilized in blocking/permeabilization buffer (2% BSA, 2% fetal bovine serum, 0.05% NP-40 in PBS) for 45 minutes and then incubated with the primary antibodies (or isotype controls). After 1 hour, the cells were washed in PBS, incubated with an Alexa-647-conjugated secondary antibody for 45 minutes, and finally washed twice with PBS. All procedures were performed at room temperature. Fluorescence-activated cell sorting analysis was carried out using a BD LSR analyzer (BD Biosciences), and data analysis was performed with the FlowJo software (Tree Star, Ashland, OR, http://www.treestar.com). The following antibodies were used in the study: anti-cardiac troponin T (Thermo Fisher Scientific, Waltman, MA, http://www.thermofisher.com), anti-sarcomeric α-actinin (Sigma-Aldrich), anti-CD31 (Invitrogen, Carlsbad, CA, http://www.invitrogen.com), anti-CD34 (Miltenyi Biotec, Bergisch Gladbach, Germany, http://www.miltenyibiotec.com), anti-smooth muscle heavy chain (Dako, Glostrup, Denmark, http://www.dako.com).

For immunofluorescence analysis, dissociated cardiomyocytes were cultured on Matrigel-coated coverslips for 4–5 days and then fixed with 3.6% paraformaldehyde. The fixed cells were permeabilized in blocking/permeabilization buffer for 45 minutes and then stained with mouse primary antibody anti-cardiac troponin T overnight at 4°C, washed three times with PBS, and then stained with Alexa Fluor-595 anti-mouse IgG for 45 minutes. Finally, the cardiomyocytes were counterstained with 4′,6-diamidino-2-phenylindole for 15 minutes. Confocal imaging was performed using a Leica SP5 confocal system (Leica, Heerbrugg, Switzerland, http://www.leica.com).

Gene Expression Analysis

Relative gene expression was determined using a two-step quantitative real-time polymerase chain reaction (PCR) method. Total RNA was isolated with the RNeasy Isolation kit with on-column DNase I treatment (Qiagen, Hilden, Germany, http://www.qiagen.com). About 1 μg total RNA was reverse transcribed using the SuperScript VILO cDNA Synthesis Kit (Life Technologies, Rockville, MD, http://www.lifetech.com). Quantitative reverse transcription PCR (RT-PCR) reactions were performed with the iTaq Fast SYBR Green Supermix (Bio-Rad, Hercules, CA, http://www.bio-rad.com) on the ABI Prism 7500 real-time PCR system (Applied Biosystems, Foster City, CA, http://www.appliedbiosystems.com). Fold changes in gene expression were determined using the comparative C_T method ($\Delta\Delta$Ct) with normalization to the housekeeping gene B2M.

Genetic Labeling of Cardiomyocytes

Single cells were plated at low density on Matrigel-coated coverslips and cultured with Dulbecco's Modified Eagle's Medium supplemented with 20% fetal bovine serum, L-glutamine (1 mM) and 1% nonessential amino acids. The next day, the cells were transduced with a recombinant lentiviral vector in which a short fragment of the human MLC2V promoter drives tdTomato expression (LV-MLC2v-tdTomato) [13].

Action Potential Recordings

Action potentials (APs) of the differentiated cells were recorded using the whole-cell configuration of the patch-clamp technique (HEKA Instruments, Bellmore, NY, http://www.heka.com) at 37°C. The current-clamp mode with 100- to 1,000-pA pulse of

5 ms delivered to the cells was used with cell capacitance and series resistance (≥70%), online compensated. AP parameters were analyzed as previously described [22]. The patch pipettes were prepared from 1.5-mm thin-walled borosilicate glass capillaries that had a typical resistance of 4–6 MΩ with an internal solution containing 110 mM K^+ aspartate, 20 mM KCl, 1 mM $MgCl_2$, 0.1 mM Na-GTP, 5 mM Mg-ATP, 5 mM Na_2-phosphocreatine, 1 mM EGTA, 10 mM HEPES, pH adjusted to 7.3 with KOH. The composition of the external Tyrode's solution was 140 mM NaCl, 5 mM KCl, 1 mM $CaCl_2$, 1 mM $MgCl_2$, 10 mM glucose, 10 mM HEPES, pH adjusted to 7.4 with NaOH.

Confocal Ca^{2+} Transient Imaging

The intracellular calcium ($[Ca^{2+}]_i$) transients were recorded by loading the cells with Fluo-3 (5μM; Invitrogen) for 30 minutes at 37°C in Tyrode's solution, followed by imaging with a spinning-disc laser confocal microscope (PerkinElmer Life and Analytical Sciences, Waltham, MA, http://www.perkinelmer.com). The electrically induced calcium (Ca^{2+}) transients were triggered by pulses generated from a field stimulator (40-ms pulse duration; 40 V/cm; 0.2 Hz), and the caffeine-induced Ca^{2+} transients were stimulated with caffeine (10 mM).

Microelectrode Array Recordings

A high-resolution microelectrode array recording system (Multi Channel Systems, Reutlingen, Germany, http://www.multichannelsystems.com) was used to characterize the electrophysiological properties of the cardiomyocytes [23]. At day 21 after differentiation, cardiomyocytes were plated on fibronectin-coated microelectrode array plates that consisted of a 50 × 50-mm glass substrate with an embedded 1.4 × 1.4-mm matrix of 60 titanium nitride-gold contact electrodes with an interelectrode distance of 200 μm. The extracellular field potentials were recorded simultaneously from all 60 electrodes and then band-pass filtered from 1 kHz to 10 kHz. Following baseline recordings, escalating doses of isoprenaline (10^{-9} mol/l to 10^{-6} mol/l) and sotalol (10^{-9} mol/l to 10^{-5} mol/l) were tested. The solution was static during the recording period, and the temperature was kept at 37°C. Data were analyzed offline to determine interspike interval and peak-to-peak amplitude (maximum and minimum) and using the MC_Rack data analysis software according to the manufacturer's instructions (Multi Channel Systems).

Optical Mapping of Membrane Potential

At 21–25 days after differentiation, cardiomyocyte monolayers were prepared by plating single-cell preparations on Matrigel-coated coverslips at a density of 10^5 cells per square centimeter. After 96 hours, the cells were incubated with the voltage-sensitive dye di-4-ANEPPS (2 mM; Life Technologies) for 10 minutes at room temperature in Tyrode's solution. The cells were stimulated with coaxial point stimulation electrodes (typically 1.5 Hz, 8 V/cm, 10-ms duration). Fluorescence images were acquired with the MiCam Ultima optical mapping system (SciMedia, Costa Mesa, CA, http://www.scimedia.com) using a 1× objective and 1× condensing lens in a 10 × 10 mm^2 field of view. Optical mapping image processing and data analysis were performed with the BV_Analyzer software (SciMedia).

Genomewide Gene Transcriptional Profiling

Differentiated cells at D4 were treated with either IWR-1 (2.5 μM) or vehicle control (dimethyl sulfoxide [DMSO]). Samples were collected at 2, 4, and 24 hours following treatment, and total RNA was isolated with the RNeasy Isolation kit (Qiagen), with on-column DNase I treatment to eliminate contaminating genomic DNA using the RNase-free DNase Set according to the manufacturer's instructions (Qiagen). The Illumina Total Prep RNA Amplification Kit (Illumina Inc., San Diego, CA, http://www.illumina.com) was used to transcribe 200 ng of total RNA to biotinynated amplified RNA according to the manufacturer's recommendation. A total of 700 ng of biotinynated amplified RNA was hybridized at 58°C for 16 hours to the Illumina HumanHT-12 v4 Expression BeadChip arrays (Illumina). The BeadChip arrays were then washed, scanned with the HiScan System (Illumina), and analyzed with the Genome Studio Software (Illumina).

Intensity values of all probes from different replicates (n = 4) were quantile normalized across multiple chips. For multiple-probe identifiers referring to a single gene, the values were averaged to calculate the mean expression value for the given gene. The differentially expressed genes between treatment and control groups at three different time points were identified with an unpaired t test (α = 5%) using MATLAB (MathWorks, Natick, MA, http://www.mathworks.com). Log2 fold changes were calculated after averaging gene expression of all different replicates. Only genes with a minimum log2 fold change of ±log2(1.3) were considered for all following analysis. The *R* library's "Venn Diagram" tool was used to generate Venn diagrams. The genes that were significantly differentially expressed and exhibited minimum fold change of ±log2(1.3) at one time point, at least, were considered for clustering with Gene Cluster 3.0 (http://bonsai.hgc.jp/~mdehoon/software/cluster/software.htm) ("Genes": "Correlation (uncentered)", "Average linkage") [24].

Biological Process Enrichment Analysis

The human gene ontology (GO) association and the full Open Biomedical Ontologies database were used for GO enrichment analysis (http://www.geneontology.org). The parent processes were populated with the genes of their children processes, as defined by the GO relationships "is_a" and "part_of." For the following enrichment analysis, all GO biological processes were considered.

Mouse target genes in the Expression2Kinases (X2K) databases [25] were replaced by their human homologs based on the Jackson Laboratories mouse informatics database (Mouse Genome Informatics [MGI], http://www.informatics.jax.org) and the National Center for Biotechnology Information homologene (http://www.ncbi.nlm.nih.gov/homologene/) database. To secure accurate computation of statistical significance, the populated GO association list and the TRANSFAC-background and ChEA-background databases were further modified. Before identification of GO biological processes or transcription factors with enriched gene targets among the differentially expressed genes, any gene target that was not on the microarray chip—and thus could not be detected as differentially expressed—was removed from the GO association list, the TRANSFAC-background, and ChEA-background database. For the identification of GO biological processes with enriched gene targets among the transcription factor intermediate networks, only gene targets that had a chance to become part of this network were kept in the GO association list. Consequently, only genes that were identified by the network

extension algorithm (described below) when using all transcription factors of the TRANSFAC-background and ChEA-background databases as seed nodes were kept in the GO association database before calculation of statistical significance for enriched processes. GO processes with only one gene association were not considered for the analysis. Similarly, differentially expressed genes or genes of the transcription factor intermediate networks that were not part of the GO association, TRANSFAC-background, or ChEA-background databases were removed before each individual analysis. The Fisher's exact test was used for enrichment analysis, and the results were ranked based on their p values. The top five TRANSFAC-background- and ChEA-background-predicted transcription factors at each time point were considered for clustering based on $-\log10(p \text{ value})$ using Gene Cluster 3.0 ("Genes": "Correlation (uncentered)", "Average linkage") [24].

Transcription Factor Intermediate Networks Analysis

The top five TRANSFAC-background-predicted and the top five ChEA-background-predicted transcription factors for each time point were used as seed nodes to generate transcription factor intermediate networks. All X2K protein-protein interaction (PPI) databases except "Predicted PPI" were chosen as the basis for the PPI network. Set to a path length of 2, the X2K network extension algorithm identifies all those genes in the PPI network, which connect at least two seed nodes (i.e., transcription factors) by a maximum path length of two edges with each other or which are seed nodes by themselves. The X2K network extension algorithm was applied using the identified 10 transcription factors as seed nodes to generate a transcription factor intermediate network for each time point. The networks were analyzed for GO biological process enrichment, as described. Only GO biological processes, which were children processes of "signal transduction" or "regulation of signaling" were considered. Networks were visualized with yED Graph Editor (yWorks GmbH, Tübingen, Germany, http://www.yworks.com/en/products_yed_about.html).

Statistical Analysis

Statistical significance was analyzed with the Student's unpaired t test. The electrophysiology data sets were analyzed using the Kolmogorov-Smirnov test. A p value of $<.05$ was considered significant.

RESULTS

Small Molecule-Mediated Directed Differentiation of hESCs

Cardiomyocyte differentiation was initiated by enzymatic dissociation of hESCs maintained in feeder-independent, serum-free culture and subsequent formation of "cardiogenic" embryoid bodies (EBs) in suspension culture in a chemically defined media. Cell viability during EB formation was enhanced by inhibition of actin-myosin contraction mediated by blebbistatin, a small molecule inhibitor of programmed cell death commonly observed in dissociated hESCs [26, 27]. Next, we combined the application of the recombinant growth factors, BMP4 and activin A, and the small molecule IWR-1, an inhibitor of the canonical Wnt pathway, in a directed differentiation protocol in two stages: In stage 1 (days 0–4.5), the hESCs were differentiated toward cardiovascular progenitors, and in stage 2 (days 4.5–8) were terminally differentiated to cardiomyocytes (supplemental online Table 1).

Molecular Analysis of Cardiomyocyte Differentiation

During differentiation in vitro, hESCs transit through a series of developmental stages that parallel those found in the embryo [28]. The protocol was refined through a time-course study using quantitative RT-PCR analysis to investigate the kinetics of gene expression of markers of pluripotency (Fig. 1A), mesoderm (Fig. 1B), primitive streak-like (Fig. 1C), cardiac mesoderm (Fig. 1D), cardiovascular progenitors (Fig. 1E–1J), and terminally differentiated cardiomyocytes (Fig. 1K–1M). In stage 1, the addition of human recombinant growth factors BMP4 and activin A induced a rapid decrease in the level of expression of NANOG (Fig. 1A), one of the key regulators of pluripotency [29], which became almost undetected by day 4.5. The expression of the transcription factor T [30] was used to monitor the onset of mesoderm induction, whereas MIXL1 [31] marked the formation of a primitive streak-like population. The activation of the BMP and nodal signaling by the addition of BMP4 and activin A, respectively, induced rapid but transient upregulation in gene expression of both T and MIXL1, which peaked at day 2 and subsequently decreased, reaching baseline levels by day 4.5 (Fig. 1B, 1C). At the same time, we detected significant upregulation of MESP1 (Fig. 1D), one of the earliest markers of cardiovascular lineage specification [32, 33]. Concomitantly, the expression levels of key cardiovascular specification genes, such as NKX2.5, GATA4, HAND1, TBX5, ISL1, and FLK1 [34], were significantly increased (Fig. 1E–1J), which signified the generation of cardiac progenitor cells. Interestingly, the transcriptional signature of $ISL1^+/NKX2.5^+/FLK1^+$ defines a multipotent cardiovascular progenitor during cardiogenesis in mice and can give rise to the major lineages of the mature heart: cardiomyocytes, endothelial cells, and smooth muscle cells [35]. Taken together, these results demonstrated that the molecular events at stage 1 of the differentiation protocol recapitulated the early stages of the cardiovascular lineage commitment.

The transcriptional analysis showed the emergence of early cardiac mesoderm population, signaled by the peak in MESP1 expression and the simultaneous upregulation of NKX2.5 and GATA-4 after the first 4.5 days of differentiation. This suggested an optimal time point for initiating the next phase of the protocol, stage 2. At this step, we treated the cells with the small molecule IWR-1, a canonical Wnt/β-catenin pathway antagonist [36]. We observed that the expression levels of NKX2.5 were progressively increased in IWR-1-treated cells, beginning on day 6 and plateauing from day 9 to day 15 (Fig. 1F). Meanwhile, the expression of *ISL1* was transiently increased from day 4.5 to day 9 but significantly decreased by day 15 in IWR-1-treated cells compared with DMSO-treated cells (Fig. 1E). There was no significant difference in the expression levels of the molecular markers of early cardiogenesis, such as GATA4 (Fig. 1I), TBX5 (Fig. 1H), and FLK1 (Fig. 1J) during the remaining course of the differentiation. Furthermore, by day 9, the results indicated that IWR-1 treatment significantly enhanced cardiogenesis, as indicated by the marked induction of the cardiac-specific genes, TNNT2 (Fig. 1K), the ventricular cardiomyocyte marker MLC2V [37] (Fig. 1L), and the ventricle-specific transcription factor IRX4 [38, 39] (Fig. 1M). Taken together, these results indicate that the timed delivery of the small molecule IWR-1 significantly enhanced the terminal differentiation of cardiac progenitors toward the cardiomyocyte lineage, recapitulating the normal human cardiac developmental scheme.

We determined that the defining step in the cardiomyocyte cell-fate determination is the immediate response on IWR-1

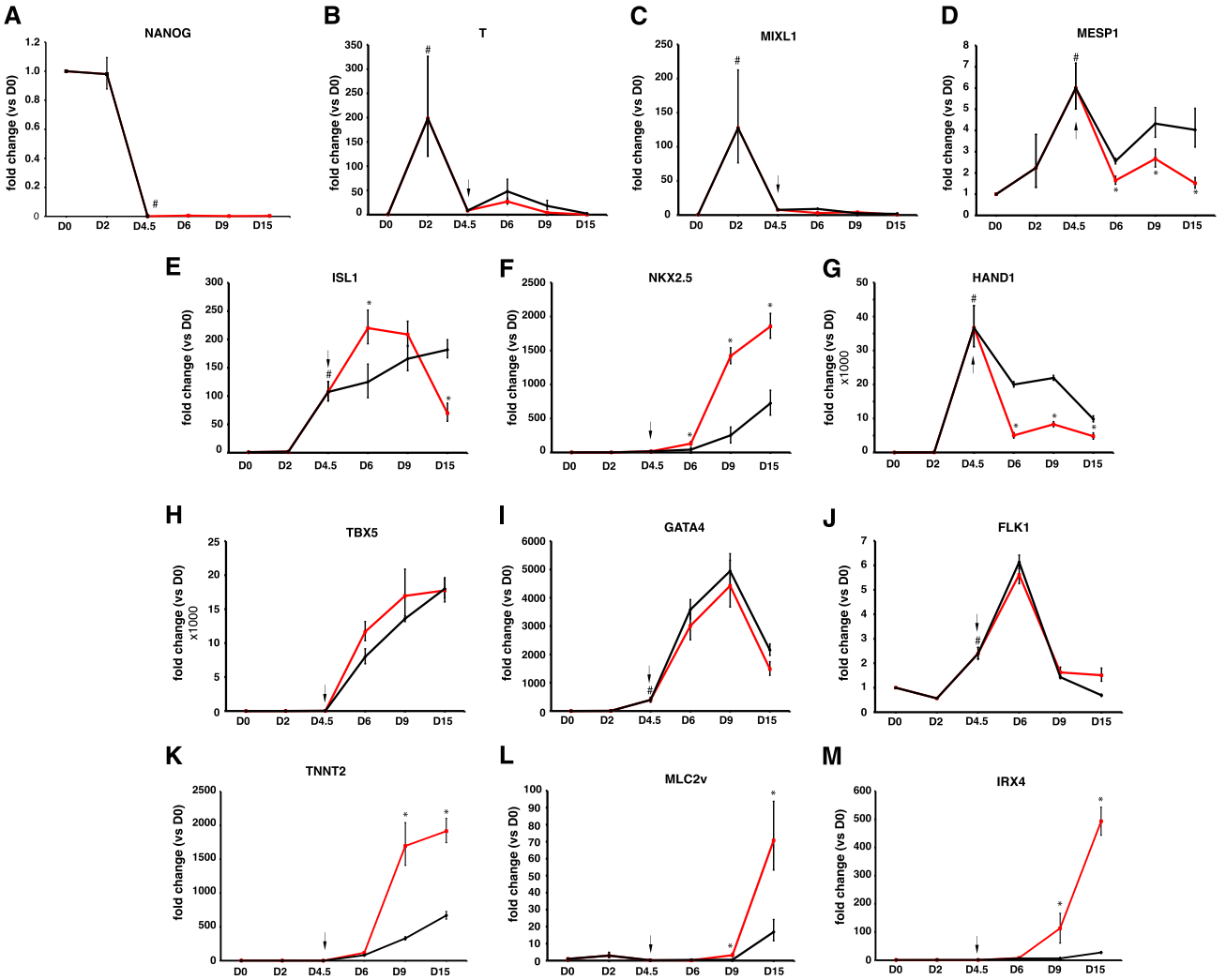

Figure 1. Molecular analysis during the course of the differentiation. Gene expression was analyzed on embryoid bodies at the indicated time points for genes associated with pluripotency **(A)**, mesoderm **(B)**, primitive streak-like **(C)**, cardiac mesoderm **(D)**, cardiac progenitors **(E–J)**, and terminally differentiated cardiomyocytes **(K–M)**. Red line: IWR-1 mediated; black line: dimethyl sulfoxide control. Arrow indicates the initiation of stage 2 of the differentiation. Gene expression was normalized to the housekeeping gene *B2M*. Values represent means ± SE of a minimum of four independent experiments. #, $p < .05$ versus D0; ∗, $p < .05$ IWR-1 versus dimethyl sulfoxide. Abbreviation: D, day.

treatment at the start of stage 2 and the inactivation of the WNT pathway as assessed by the phosphorylation of β-catenin (supplemental online Fig. 1). Consequently, we further explored the temporal dynamics of cardiac fate determination by obtaining the genome-wide mRNA expression profiles of differentiating cells at 2, 4, and 24 hours following IWR-1 treatment. We identified 673 downregulated genes and 849 upregulated genes in the IWR-1 compared with the DMSO-treated cells at the three time points examined (supplemental online Table 2, supplemental online Fig. 2). The expression levels of these genes over the three time points were clustered by expression pattern using Gene Cluster 3.0 (Fig. 2A).

To gain broader insights into the molecular pathways associated with differentially expressed genes, we determined the GO biological processes that were enriched for the differentially expressed genes and ranked them based on their *p* values. Enrichment analysis indicated that the upregulated genes at 2 hours were significantly enriched for genes involved in "Wnt receptor signaling" (Fig. 2B), whereas at 4 hours, the top process in the downregulated gene set was the "cardiac epithelial-to-mesenchymal transition" (supplemental online Fig. 3). At 24 hours, upregulated genes were significantly enriched for "cardiomyocyte differentiation" terms, including "cardiac muscle cell differentiation," further supporting that IWR-1 treatment drives cardiomyocyte cell differentiation (supplemental online Fig. 3). Accordingly, individual expression levels for key genes of interest were plotted as a function of time to highlight the transcriptional regulation of genes associated with Wnt signaling, epithelial-to-mesenchymal transition, and cardiomyocyte and noncardiomyocyte cell differentiation (supplemental online Fig. 4).

Next, we used computational approaches to identify potential upstream regulatory mechanisms that are responsible for observed changes in gene expression based on two transcription factor gene target association databases of the X2K suite [25]. We identified 10 transcription factors at each time point as putative upstream regulators of the identified differentially expressed gene sets (Fig. 2C). Using these transcription factors as seed nodes in the human interactome, a transcription factor

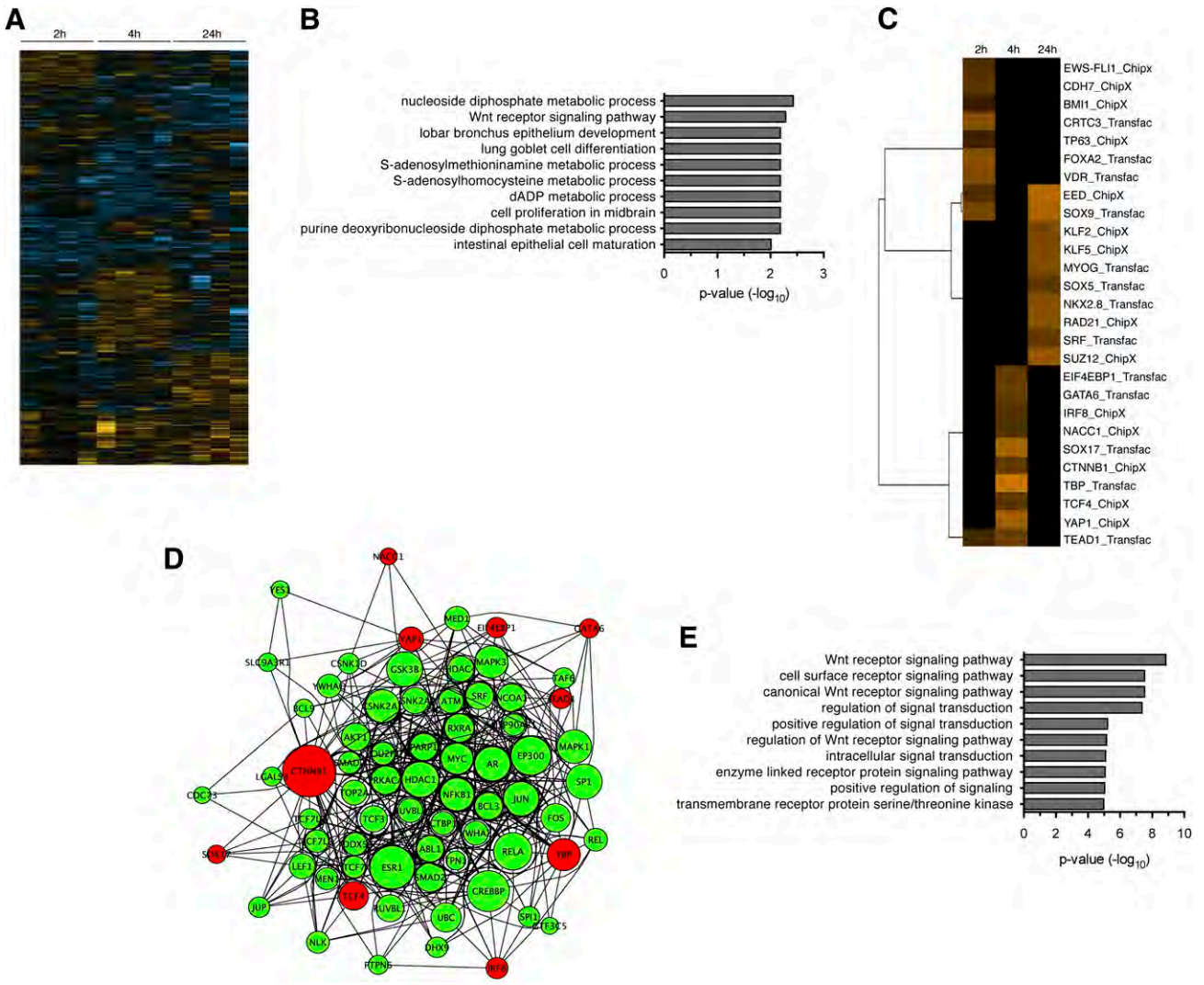

Figure 2. Transcriptional profiling and system biology analyses at the initiation of stage 2. **(A):** The differentially expressed genes in IWR-1 compared with dimethyl sulfoxide-treated cells were clustered by expression pattern at the indicated time points. **(B):** The up- and downregulated genes at the indicated time points were analyzed for gene ontology (GO) biological process enrichment. **(C):** The top 10 transcription factors as putative upstream regulators at each time point were identified with the Expression2Kinases suite. **(D):** The predicted transcription factors of each time point were used as seed nodes to generate transcription factor networks. The protein-protein interaction network at 4 hours is shown. **(E):** The transcription factor regulatory networks were analyzed for GO process enrichment. Only signaling processes (i.e., subprocesses of the GO processes "signaling" and "regulation of signaling") are shown. Abbreviation: dADP, deoxyadenosine diphosphate.

intermediate network was generated for each time point (Fig. 2D; supplemental online Fig. 5). The networks were analyzed for GO biological process enrichment to identify signaling mechanisms regulating these networks. The identified signaling GO terms were ranked based on their *p* values. Among the top 10 signaling-related processes of the 4-hour transcription factor network were three processes related to (canonical) Wnt receptor signaling, with "Wnt receptor signaling" ranked first; the other seven processes referred to unspecific signaling processes (Fig. 2E). Our results are in agreement with the pivotal role of Wnt signaling in cardiomyocyte development. Furthermore, the activity of the Wnt receptor signaling pathway is one of the major switches that regulates cardiomyocyte cell fate, suggesting that Wnt signaling inhibition by IWR-1 is the mechanism of action.

Taken together, these results indicate that the small molecule IWR-1 regulates gene expression programs that promote commitment toward the cardiomyocyte lineage by inhibiting the Wnt signaling pathway.

Cardiomyocyte Differentiation Efficiency

Initially, the cardiomyocyte differentiation efficiency was assessed based on the spontaneous contractile activity. The earliest spontaneously beating activity in IWR-1-treated cells was observed at day 7. The number of spontaneously contracting EBs significantly increased from ~8% at day 7 to nearly 100% by day 15 (supplemental online Fig. 6, supplemental online Movie 1). In contrast, a modest proportion of beating EBs (~10%) was observed in the control-treated cultures (supplemental online Fig. 6A). In addition, we demonstrated that the timing of the initiation of stage 2 significantly affected the differentiation efficiency, suggesting that the optimal time window for the

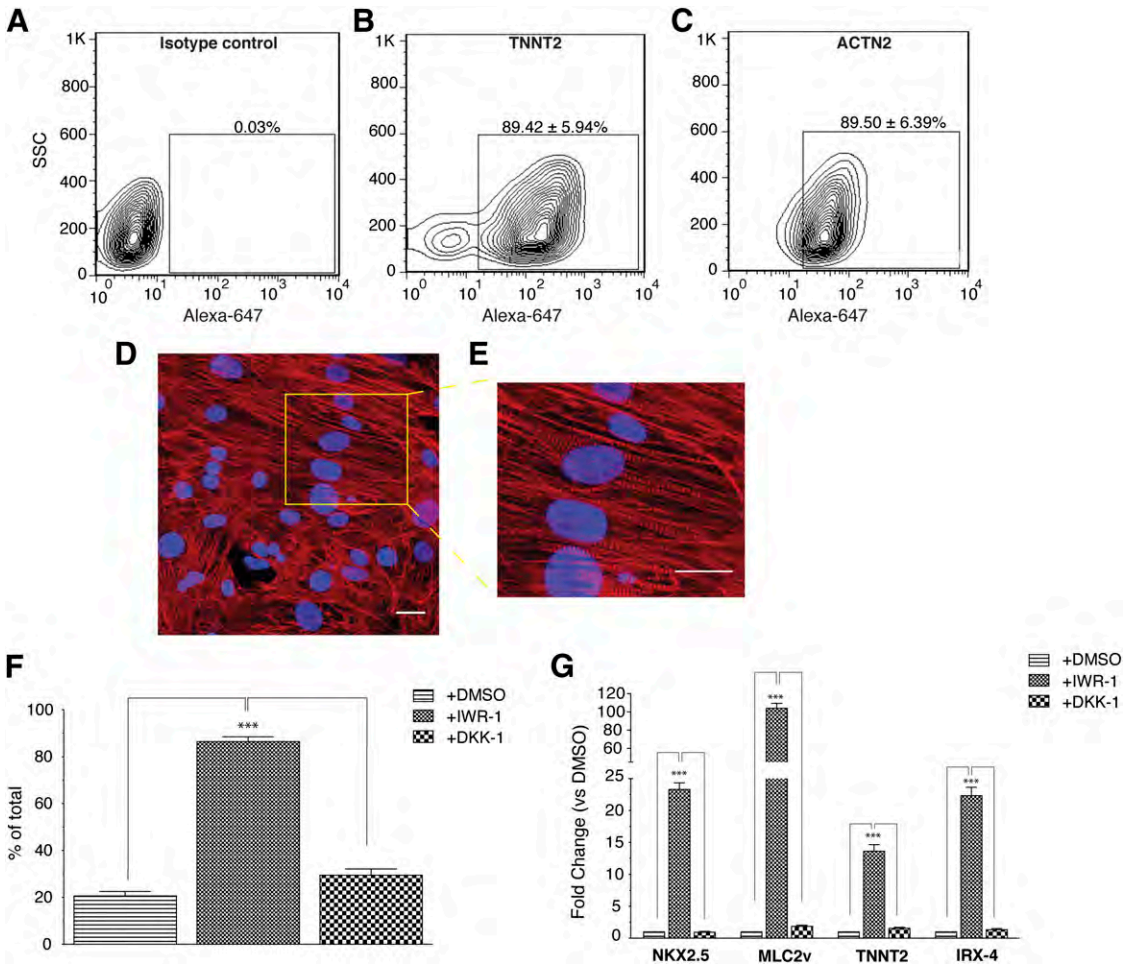

Figure 3. Quantification of the cardiomyocyte differentiation efficiency. **(A–C):** Flow cytometry analysis of the differentiation efficiency of at 21 days after differentiation. Representative contour plots of cells immune labeled with antibodies against the IgG isotype control antibody **(A)** or the cardiomyocyte marker genes *TNNT2* **(B)** or *ACTN2* **(C)**. Values represent means ± SE of six independent differentiation experiments. Alexa Fluor-647 indicates the secondary antibody fluorescence. **(D, E):** Structural organization of cardiomyocytes. Representative immunofluorescence staining images of the cardiomyocyte-specific marker *TNNT2* (red); DNA was counterstained with 4′,6-diamidino-2-phenylindole (blue) **(D)**. The high magnification of the indicated region shows that the cardiomyocytes have well-organized myofilament structures **(E)**. Scale bar = 20 μm. **(F, G):** Comparison of the cardiomyocyte differentiation efficiency in the current protocol (IWR-1) and the protocol described by Yang et al. [6] (DKK1). Flow cytometric quantification of the percentage of *TNNT2*-expressing cells treated with IWR-1 or DKK1 or in the absence of either inhibitor (DMSO) **(F)**. Quantitative reverse transcription polymerase chain reaction expression analysis of the cardiomyocyte marker genes *NKX2.5*, *TNNT2*, *MLC2v*, and *IRX4* **(G)**. Gene expression was normalized to *B2M* endogenous control. Values represent means ± SE of a minimum of four independent experiments. ∗, $p < .001$. Abbreviations: DMSO, dimethyl sulfoxide; SSC, side scatter.

inhibition of the WNT pathway is relatively short (supplemental online Fig. 6B). At day 21, we determined the cardiomyocyte differentiation efficiency by fluorescence-activated cell sorting analysis. The results showed that there was a high proportion of cardiomyocytes, as assessed by the expression of the cardiomyocyte-specific markers TNNT2 (89.42 ± 5.94%) and a-sarcomeric actinin (ACTN2; 89.50 ± 6.39%) (Fig. 3A–3C). In addition, immunofluorescence staining of TNNT2 confirmed the purity of the cardiomyocytes, which displayed well-organized sarcomeres (Fig. 2D, 2E).

We next investigated whether the two-stage protocol was more efficient than existing methods for the differentiation of hESCs toward cardiomyocytes. To this end, we performed a comparison of our protocol (i.e., IWR-1) and the protocol described by Yang et al. [6] (i.e., DKK1), which utilized a cocktail of cytokines including the recombinant protein DKK1, a secreted factor that functions as a negative regulator of the canonical Wnt signaling [40]. We used phenotypic and molecular analyses in order to compare the populations derived by the two different protocols. By flow cytometry, we observed a significant increase in the cardiomyocyte differentiation efficiency of IWR-1-treated cells ($n = 6$) when compared with DKK1-treated cells ($n = 4$), as assessed by *TNNT2* expression (89.42 ± 5.94% vs. 29.48 ± 2.49%, $p = .001$) (Fig. 3F). In the absence of either inhibitor, TNNT2 was expressed in 20.64 ± 3.79% ($n = 4$) of the cells at the end of the protocol (Fig. 3F). Furthermore, we assessed the gene expression of cardiomyocyte markers at day 21 after differentiation by quantitative RT-PCR. The analysis revealed that there was a significant increase in mRNA transcript levels of the cardiomyocyte-specific genes TNNT2 (9-fold, $p < .001$), NKX2.5 (26-fold; $p < .001$), IRX4 (17-fold: $p < .001$) and MLC2v (56-fold; $p < .001$) in the IWR-1-treated cells when compared with DKK1-treated cells (Fig. 3G).

To determine whether other cardiovascular lineages were generated at the end of our protocol, we performed analysis for specific markers of smooth muscle and endothelial cells by flow cytometry (supplemental online Fig. 7). The results suggested that ~7% of the population expressed the smooth muscle heavy chain protein (MYH11) (supplemental online Fig. 7A, 7B), a structural protein that is a major component of the contractile apparatus specifically expressed in smooth muscle cells [41]. We also analyzed the expression of the CD31 and CD34 markers that are typically associated with vascular endothelial cells and were found to be expressed in ~1% of the differentiated population (supplemental online Fig. 7C, 7D).

To further validate our method, we evaluated the cardiomyocyte differentiation efficiency of our protocol in three additional lines: H7 (WA07) and H1 (WA01) hESC lines and the SKiPS-31.3 iPSC line that was derived from human dermal fibroblasts. Under the same differentiation conditions developed in the HES2 line, the H7 cells generated >90% and the H1 line generated >80% cardiomyocytes, as assessed by flow cytometric analysis of TNNT2 and ACTN2 expression (supplemental online Fig. 8). Similarly, when the protocol was applied to the SKiPS-31.3 cells, a high proportion of TNNT2-positive or ACTN2-positive cells (>90%) was observed (supplemental online Fig. 9, supplemental online Movie 2).

Taken together, these results demonstrate that the small molecule-mediated directed differentiation protocol generated a nearly pure population of cardiomyocytes with few non-cardiomyocyte cells, such as smooth muscle and endothelial cells, presented in the cell population.

Electrophysiological Characterization

The existing differentiation protocols generate a population of heterogeneous cardiomyocytes that are classified into atrial-like, ventricular-like, or nodal-like subtypes based on their electrophysiological properties. We utilized the patch-clamp method to analyze the AP and electrophysiological properties of the cardiomyocytes generated in our protocol. The AP waveforms were classified into atrial-like, ventricular-like, or nodal-like cell types based on the AP parameters (the complete set of criteria is presented in supplemental online Table 3). Electrophysiological characterization of AP recordings from single cells revealed a homogeneous AP phenotype with 100% of the cells displaying the typical ventricular-like AP parameters (Fig. 4A, 4B; supplemental online Table 4). No atrial-like or nodal-like subtypes were observed. Moreover, the AP parameters displayed by these chemically induced VCMs (ciVCMs) were comparable to cultured fetal ventricular cardiomyocytes [8] and expressed the major cardiac ion-channel genes hERG, CACNA1C, and SCN5 (supplemental online Fig. 10).

We also evaluated the electrophysiological properties of cardiomyocytes derived from the H7 hESC line. The analysis of the AP parameters obtained from single H7-derived cardiomyocytes revealed a homogeneous population of VCMs (supplemental online Fig. 11, supplemental online Table 5). These results demonstrated that that the ventricular specification of the cardiomyocytes derived with our protocol was not caused by an intrinsic propensity of the HES2 line used in the development of the protocol.

Furthermore, we evaluated the electrophysiological properties of the ciVCMs at the multicellular level using an optical mapping technique [23] (Fig. 4C–4F) by generating ciVCM monolayers (supplemental online Movie 3). Consistent with single-cell patch-clamp analysis, the AP recordings obtained from distal sites on confluent monolayers of ciVCMs displayed morphologies that resembled each other (Fig. 4D), and the AP duration at 90% repolarization (APD_{90}) was unimodally distributed, indicating a homogeneous population. The analysis of the isochronal conduction contour map of the same preparation (Fig. 4C) demonstrated that the propagation of the depolarizing wavefront had a conduction velocity of 2.15 $\pm$ 0.35 cm per second.

To corroborate the ventricular-like phenotype, we performed electrophysiological recordings of single-cell preparations labeled with a genetic marker of the ventricular fate. The ciVCMs were transduced with a recombinant lentiviral vector in which a short fragment of the MLC2v promoter [13, 37] drives the expression of tdTomato. We observed that all of the tdTomato-positive cells exhibited ventricular-like AP waveforms (supplemental online Fig. 12).

To further demonstrate that the current protocol enhances the differentiation of VCMs, we compared the electrophysiological properties of the cardiomyocytes generated with the current protocol and those generated as described by Yang et al. [6]. The cardiomyocyte phenotypes were classified as nodal-like, atrial-like, or ventricular-like based on the AP morphology and parameters. Electrophysiological characterization of individual cells using the patch-clamp method showed that the DKK1 protocol generated a heterogeneous population consisting of atrial-like, ventricular-like, and nodal-like phenotypes, whereas all the cardiomyocytes derived with the IWR-1 protocol were classified as ventricular-like (Fig. 5A, 5B; supplemental online Fig. 13). In addition, we performed a frequency distribution analysis of the AP parameters of the individual cardiomyocytes that were differentiated with either the IWR-1 or the DKK1 protocol. The frequency distribution of the APD_{90} (Fig. 4C, 4D) and the AP amplitude (APA) (Fig. 5E, 5F) were significantly different between the IWR-1 and DKK1 protocols (APD_{90}: $p = .001$; APA: $p = .04$; Kolmogorov-Smirnov test). In the IWR-1 protocol, we observe that the APD_{90} and APA values were unimodally distributed (Fig. 5C, 5E). In contrast, the DKK1-differentiated population appeared multimodally distributed.

These data demonstrate that the small molecule-mediated directed differentiation of hESCs promotes the ventricular specification of the hESC-derived cardiomyocytes.

Functional Characterization of ciVCMs

For chemically derived cardiomyocytes to be useful, it is important to examine their functional properties beyond the expression of cardiomyocyte-specific molecular markers. Thus, we assessed the Ca^{2+}-handling properties and the β-adrenergic receptor signaling responses of the ciVCMs.

Ca^{2+} homeostasis is crucial for excitation-contraction coupling and, subsequently, the contractile properties of functional cardiomyocytes [42]. We assessed whether excitation-contraction coupling was dependent on Ca^{2+} signaling by examining the $[Ca^{2+}]_i$ transients using fast line-scan confocal imaging on ciVCMs loaded with the Ca^{2+} indicator Fluo-3. The analysis revealed rhythmical Ca^{2+} transients recorded from electrically stimulated ciVCMs (Fig. 6A). We also tested for caffeine responsiveness, an indicator of functional sarcoplasmic reticulum. Caffeine application elicited a rapid release of Ca^{2+} from intracellular stores (Fig. 6B), characterized by a larger Ca^{2+} amplitude transient compared with

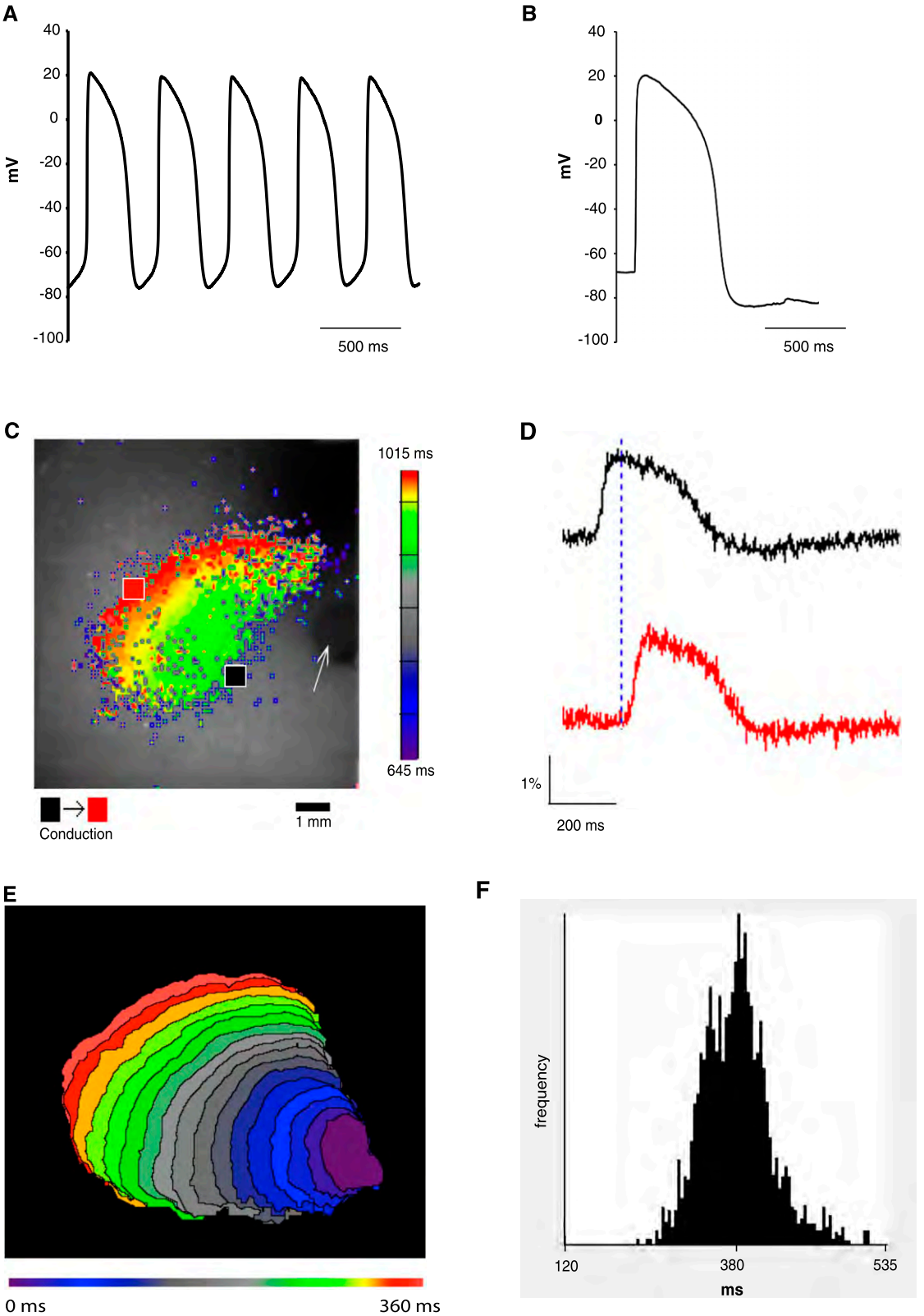

Figure 4. Electrophysiological characterization. The action potential (AP) properties of single cells were analyzed using the patch-clamp method. **(A, B):** Representative AP waveforms of spontaneous **(A)** and electrically stimulated **(B)** cells indicating a ventricular-like phenotype. Electrophysiological properties at the multicellular level: Single-cell preparations were plated at high density to form a monolayer and were stained with the voltage-sensitive dye di-4-ANNEPS for high-resolution optical mapping. **(C, D):** Representative AP tracings **(D)**, which were mapped from two sites distal to the unipolar pacing electrode (indicated by the arrow) that correlates with the two designated points (black and red) in the representative pseudocolor repolarization map recorded from a monolayer **(C)**. The conduction velocity was calculated based on the distance between the two points and the conduction time delay,

(*Figure legend continues on next page.*)

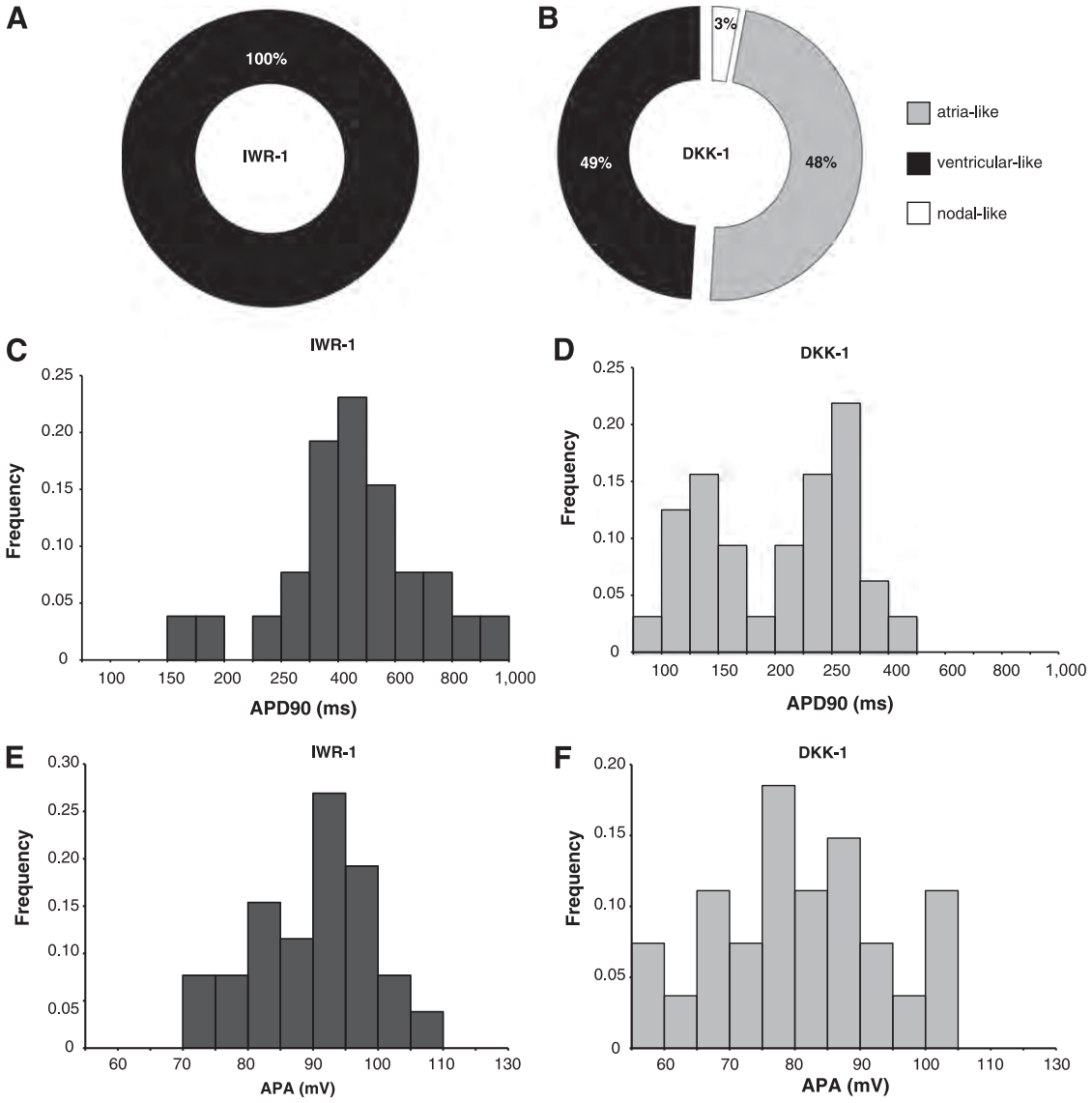

Figure 5. Electrophysiological properties of the cardiomyocytes generated with two different protocols. Directed cardiomyocyte differentiation experiments were performed with the current protocol (IWR-1) and the method described by Yang et al. [6] (DKK1). **(A, B):** Doughnut charts showing the proportion of cardiomyocytes that were classified as atrial-, ventricular- and nodal-like subtypes in the IWR-1 protocol ($n = 26$) **(A)** and the DKK1 protocol ($n = 31$) **(B)**. All cells in the IWR-1 protocol were classified as ventricular-like, whereas the DKK1 protocol generated a heterogeneous population consisting of atrial-like (48%), ventricular-like (49%), and nodal-like cardiomyocytes (3%). **(C–F):** Frequency distributions of the individual action potential values obtained from single cells in the indicated protocols. Frequency distribution of the APD90 parameters **(C, D)** and the APA parameters **(E, F)**. The distributions were significantly different in the IWR-1 protocol when compared with the DKK1 protocol (APD90: $p = .001$; APA: $p = .04$; Kolmogorov-Smirnov test). Abbreviations: APA, action potential amplitude; APD90, action potential duration at 90% repolarization.

nonstimulated cells (1.24 ± 0.13 vs. 1.69 ± 0.25; $p < .05$) (Fig. 6C) and a significant increase in the maximum upstroke velocity (2.88 ± 0.69 vs. 2.18 ± 0.24 s^{-1}; $p < .05$) (Fig. 6D) and maximum decay velocity (1.31 ± 0.40 vs. 1.11 ± 0.15 s^{-1}; $p < .05$) (Fig. 6E).

The β-adrenergic signaling cascade is an important regulator of myocardial function, which serves as the most powerful regulatory mechanism to enhance myocardial performance in response to stress or exercise [43]. A positive ionotropic response to β-adrenergic stimulation requires appropriate surface membrane receptors coupled to a signaling pathway that stimulates the appropriate ion channels, receptors, and myofilament proteins. Gene expression analysis confirmed that both β-1 and β-2 adrenergic receptors (also known as *ADRB1* and *ADRB2*, respectively) were expressed in the ciVCMs (data not shown). On isoproterenol stimulation, the ciVCMs produced a positive response in a dose-dependent manner, whereas sotalol, a β-adrenergic antagonist, negatively affected the beating rate (Fig. 6F–6J). These results demonstrate the

(*Figure legend continued from previous page.*)
yielding an overall speed of 2.15 ± 0.35 cm per second (mean $\pm$ SE of five independent experiments). **(E):** Representative isochrones map with 18-ms intervals shows a circular spreading pattern of the optically mapped transmembrane potentials. **(F):** Histogram shows the distribution of the AP duration at 90% repolarization values that were calculated from 755 spatially distinct locations from five monolayers.

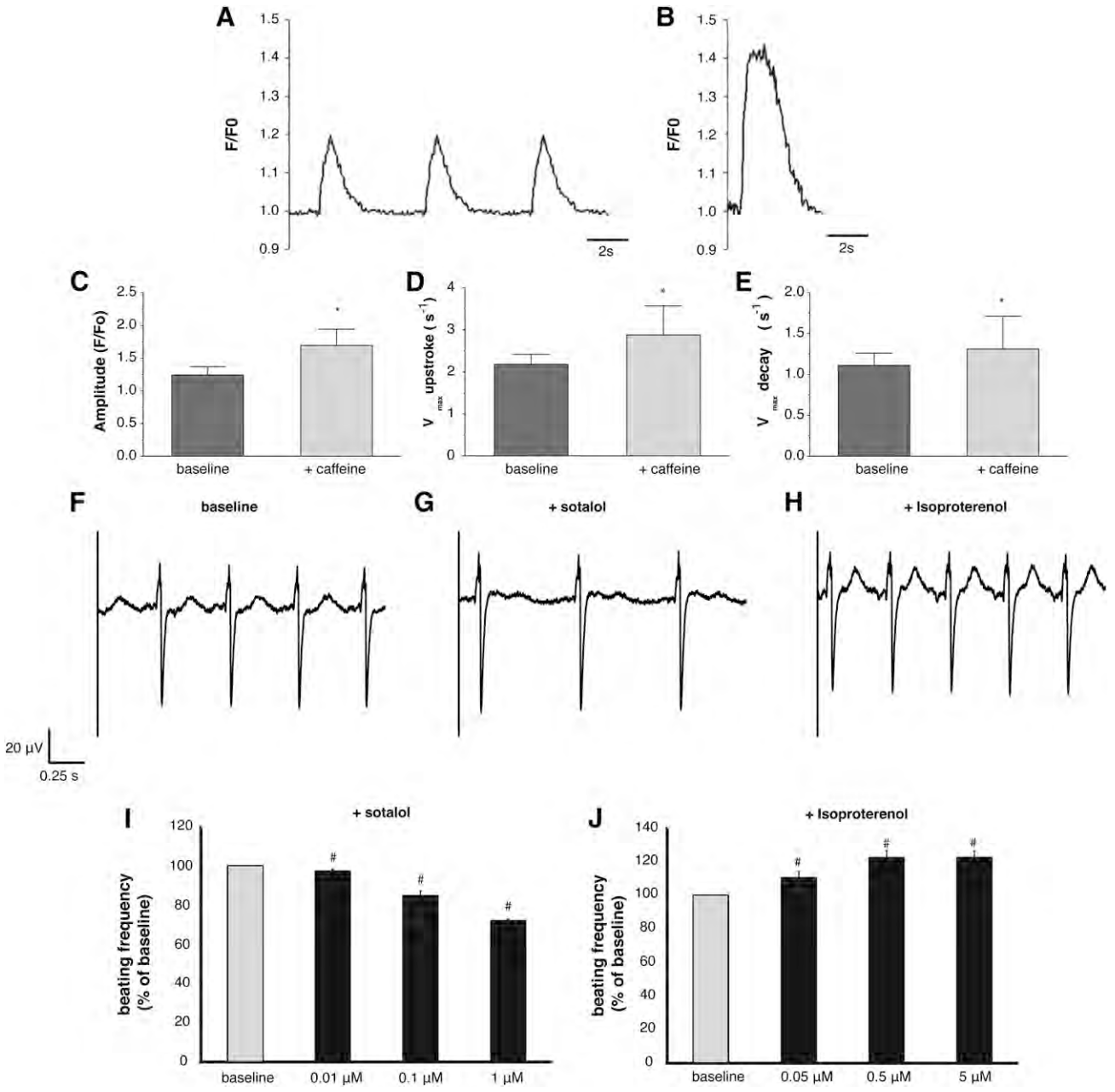

Figure 6. Functional characterization of the chemically induced VCMs (ciVCMs). **(A, B):** Intracellular calcium ($[Ca^{2+}]_i$) transient recordings in ciVCMs. Single-cell preparations were loaded with a fluorescent calcium-sensitive dye (Fluo-4), and calcium transients were recorded in a spinning disk laser confocal microscope utilizing the line-scan mode. Representative $[Ca^{2+}]_i$ transient line-scan tracing recorded from an electrically induced (0.2 Hz) ciVCM **(A)** and during the response to rapid administration of 10 mM of caffeine **(B)**. **(C–E):** Effect of caffeine application (10 mM) on $[Ca^{2+}]_i$ transient parameters. Analyses of $[Ca^{2+}]_i$ transient amplitude **(C)**, upstroke velocity **(D)**, and upstroke decay velocity **(E)**. Values represent means ± SE of $n = 28$ (baseline) and $n = 13$ (caffeine). ∗, $p < .05$ versus the baseline values. **(F–J):** Chronotropic responses of ciVCMs to cardioactive compounds: representative extracellular field potential recordings at baseline **(F)**, after administration of 1 μM of sotalol **(G)**, and 5 μM of isoproterenol **(H)**. Dose-response histograms showing the percentage of change in spontaneously beating rate on administration of escalating concentrations (0.01 μM, 0.1 μM, and 1 μM; $n = 12$) of sotalol **(I)** and of isoproterenol (0.05 μM, 0.5 μM, and 5 μM; $n = 12$) (**J**), relative to baseline conditions (100%). Values represent means ± SE. #, $p < .01$ versus the baseline values. Abbreviation: F/F0, fluorescence normalized to baseline fluorescence.

presence and functionality of the β-adrenergic receptor-signaling pathway in the ciVCMs.

Discussion

A better understanding of the signaling pathways during development has led to the development of assays to control cardiomyocyte specification in vitro; however, the current protocols are producing a heterogeneous population of cardiomyocytes, suggesting the necessity of further refinement. In this study, we describe a fully chemically defined, two-step differentiation protocol using a combination of recombinant growth factors and small molecules that efficiently promotes the differentiation of hESCs toward VCMs at the expense of other

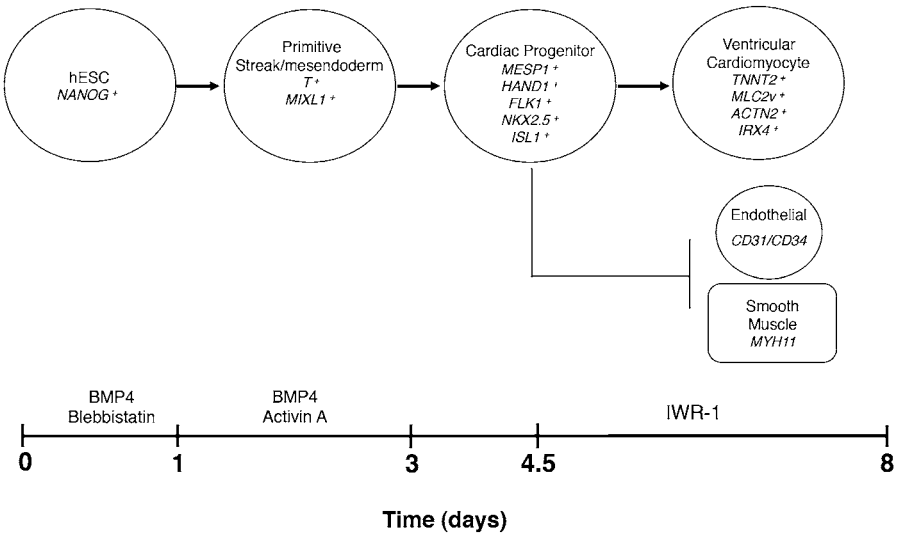

Figure 7. Schematic representation of the directed differentiation protocol in two stages. In stage one (days 0–4.5), the hESCs grown in feeder-independent conditions were differentiated toward a multipotent cardiovascular progenitor population by the combinatorial activation of the BMP and nodal/activin signaling pathways. In stage 2 (days 4.5–8), the uncommitted progenitors were terminally differentiated toward ventricular-like cardiomyocytes by the inhibition of the WNT signaling pathway with the small molecule IWR-1. Abbreviations: BMP, bone morphogenic proteins; hESC, human embryonic stem cell.

mesoderm-derived lineages, such as endothelial and smooth muscle (Fig. 7). The successful incorporation of small molecules into the protocol provides a reproducible, cost-effective, and scalable assay, generating a homogeneous population of VCMs.

In this study, cardiac differentiation was initiated by formation of EBs in suspension culture from hESCs that maintained in feeder-independent and serum-free conditions. The EBs were formed in the presence of the small molecule blebbistatin, a myosin inhibitor known to efficiently suppress the dissociation-induced apoptosis of hESCs [26, 27]. As a result of the blebbistatin treatment, apoptosis was inhibited and EB formation efficiency was significantly increased. In the first phase of the differentiation process (stage 1), the cells were differentiated into primitive streak-mesendoderm and subsequently to cardiac mesoderm by the combinatorial activation of the BMP and nodal/activin signaling pathways. In the second phase (stage 2), the inhibition of the Wnt/β-catenin pathway by the small molecule IWR-1 [36] enhanced the differentiation of the cardiac progenitors to the ventricular cardiomyocyte lineage. The two-step protocol was highly efficient, with ~90% of the differentiated population expressing cardiomyocyte-specific markers. The enhanced differentiation efficiency of the protocol was confirmed in multiple hESC lines and in a patient-specific iPSC line. The cardiomyocytes produced with this protocol display the characteristics of the ventricular-like subtype as assessed by their electrophysiological phenotype. In addition, the ciVCMs displayed functional Ca^{2+} handling properties and exhibited physiological responses to cardioactive compounds.

Moreover, the utilization of small molecules in the generation of specialized cell populations under defined conditions in vitro could provide a chemical genetics-based interrogation of signaling pathway functions during cardiogenesis that bypasses the limitations of genetic approaches. Recent studies revealed the importance of the canonical Wnt/β-catenin pathway in cardiac differentiation and development [44–46]. Using an integrated computational and experimental systems biology approach, we demonstrated that the temporal inhibition of the Wnt/β-catenin pathway by the small molecule IWR-1 is also critical for the specification of hESC-derived cardiovascular progenitor cells toward the ventricular cardiomyocyte cell fate. Our findings are further supported by a recent study that showed the disruption of atrium formation in zebrafish embryos treated with IWR-1 after gastrulation, resulting in the formation of a single ventricular chamber [47].

The delineation of the Wnt/β-catenin signaling pathway during cardiogenesis in vitro by utilizing small molecules, such as IWR-1, could provide important insights into the molecular mechanisms that regulate cardiomyocyte subtype specification during development in the human heart. The phenotypic differences observed between cardiovascular progenitors treated with IWR1 and those treated with DKK1 suggest that the cardiomyocyte subtype specification during development is controlled by intrinsic differences among Wnt signaling components. The further elucidation of the molecular mechanisms that underlie cardiomyocyte subtype specification is essential to improve our understanding of cardiovascular development and is expected to translate into applied research, drug development, and, ultimately, regenerative therapies. We may be able to regulate the commitment, proliferation, and differentiation of pluripotent stem cells into ventricular cardiomyocytes and harness these cells for therapeutic purposes.

Conclusion

Our ventricular cardiomyocte differentiation system provides a reproducible and efficient experimental platform that could advance basic developmental research, facilitate large-scale pharmacological screening, and provide a valuable source of ventricular cardiomyocytes for cell replacement therapies.

Acknowledgments

This work is supported by NIH R01 HL093183, HL088434, P20HL100396, a National Heart, Lung, and Blood Institute Program of Excellence in Nanotechnology (PEN) award, contract

no. HHSN268201000045C, and P50 HL112324. I.K. is currently affiliated with the Division of Cardiovascular Medicine, Department of Medicine, Stanford University School of Medicine, Stanford University, Stanford, CA.

Author Contributions

I.K.: conception and design, collection and assembly of data, data analysis and interpretation, manuscript writing, final approval of manuscript; G.D.S.: conception and design, collection and assembly of data, data analysis and interpretation, manuscript writing; J.H.: data analysis and interpretation, manuscript writing; C.-W.K.: collection and data analysis; E.U.A., D.K.L., J.-S.H., R.I., and R.A.L.: data analysis and interpretation; F.S., J.W., and L.R.: collection and assembly of data; R.J.H.: conception and design, financial support, final approval of manuscript.

Disclosure of Potential Conflicts of Interest

J.-S.H. has compensated research funding.

References

1 Evans SM, Yelon D, Conlon FL et al. Myocardial lineage development. Circ Res 2010; 107:1428–1444.

2 Olson EN. Gene regulatory networks in the evolution and development of the heart. Science 2006;313:1922–1927.

3 Noseda M, Peterkin T, Simões FC et al. Cardiopoietic factors: Extracellular signals for cardiac lineage commitment. Circ Res 2011;108: 129–152.

4 Kehat I, Kenyagin-Karsenti D, Snir M et al. Human embryonic stem cells can differentiate into myocytes with structural and functional properties of cardiomyocytes. J Clin Invest 2001;108:407–414.

5 Laflamme MA, Chen KY, Naumova AV et al. Cardiomyocytes derived from human embryonic stem cells in pro-survival factors enhance function of infarcted rat hearts. Nat Biotechnol 2007;25:1015–1024.

6 Yang L, Soonpaa MH, Adler ED et al. Human cardiovascular progenitor cells develop from a KDR+ embryonic-stem-cell-derived population. Nature 2008;453:524–528.

7 He JQ, Ma Y, Lee Y et al. Human embryonic stem cells develop into multiple types of cardiac myocytes: Action potential characterization. Circ Res 2003;93:32–39.

8 Mummery C, Ward-van Oostwaard D, Doevendans P et al. Differentiation of human embryonic stem cells to cardiomyocytes: Role of coculture with visceral endoderm-like cells. Circulation 2003;107:2733–2740.

9 Xu C, Police S, Rao N et al. Characterization and enrichment of cardiomyocytes derived from human embryonic stem cells. Circ Res 2002;91:501–508.

10 Burridge PW, Thompson S, Millrod MA et al. A universal system for highly efficient cardiac differentiation of human induced pluripotent stem cells that eliminates interline variability. PLoS One 2011;6:e18293.

11 Anderson D, Self T, Mellor IR et al. Transgenic enrichment of cardiomyocytes from human embryonic stem cells. Mol Ther 2007;15: 2027–2036.

12 Kita-Matsuo H, Barcova M, Prigozhina N et al. Lentiviral vectors and protocols for creation of stable hESC lines for fluorescent tracking and drug resistance selection of cardiomyocytes. PLoS One 2009;4:e5046.

13 Huber I, Itzhaki I, Caspi O et al. Identification and selection of cardiomyocytes during human embryonic stem cell differentiation. FASEB J 2007;21:2551–2563.

14 Ao A, Hao J, Hong CC. Regenerative chemical biology: Current challenges and future potential. Chem Biol 2011;18:413–424.

15 Wu X, Ding S, Ding Q et al. Small molecules that induce cardiomyogenesis in embryonic stem cells. J Am Chem Soc 2004;126: 1590–1591.

16 Takahashi T, Lord B, Schulze PC et al. Ascorbic acid enhances differentiation of embryonic stem cells into cardiac myocytes. Circulation 2003;107:1912–1916.

17 Sadek H, Hannack B, Choe E et al. Cardiogenic small molecules that enhance myocardial repair by stem cells. Proc Natl Acad Sci USA 2008;105:6063–6068.

18 Diamandis P, Wildenhain J, Clarke ID et al. Chemical genetics reveals a complex functional ground state of neural stem cells. Nat Chem Biol 2007;3:268–273.

19 Borowiak M, Maehr R, Chen S et al. Small molecules efficiently direct endodermal differentiation of mouse and human embryonic stem cells. Cell Stem Cell 2009;4:348–358.

20 Galende E, Karakikes I, Edelmann L et al. Amniotic fluid cells are more efficiently reprogrammed to pluripotency than adult cells. Cell Reprogram 2010;12:117–125.

21 Ludwig TE, Bergendahl V, Levenstein ME et al. Feeder-independent culture of human embryonic stem cells. Nat Methods 2006;3:637–646.

22 Moore JC, Fu J, Chan YC et al. Distinct cardiogenic preferences of two human embryonic stem cell (hESC) lines are imprinted in their proteomes in the pluripotent state. Biochem Biophys Res Commun 2008;372:553–558.

23 Weinberg S, Lipke EA, Tung L. In vitro electrophysiological mapping of stem cells. Methods Mol Biol 2010;660:215–237.

24 de Hoon MJ, Imoto S, Nolan J et al. Open source clustering software. Bioinformatics 2004; 20:1453–1454.

25 Chen EY, Xu H, Gordonov S et al. Expression2Kinases: mRNA profiling linked to multiple upstream regulatory layers. Bioinformatics 2012; 28:105–111.

26 Chen G, Hou Z, Gulbranson DR et al. Actinmyosin contractility is responsible for the reduced viability of dissociated human embryonic stem cells. Cell Stem Cell 2010;7:240–248.

27 Ohgushi M, Matsumura M, Eiraku M et al. Molecular pathway and cell state responsible for dissociation-induced apoptosis in human pluripotent stem cells. Cell Stem Cell 2010;7:225–239.

28 Keller GM. In vitro differentiation of embryonic stem cells. Curr Opin Cell Biol 1995;7: 862–869.

29 Jaenisch R, Young R. Stem cells, the molecular circuitry of pluripotency and nuclear reprogramming. Cell 2008;132:567–582.

30 Kispert A, Herrmann BG, Leptin M et al. Homologs of the mouse Brachyury gene are involved in the specification of posterior terminal structures in Drosophila, Tribolium, and Locusta. Genes Dev 1994;8:2137–2150.

31 Ng ES, Azzola L, Sourris K et al. The primitive streak gene Mixl1 is required for efficient haematopoiesis and BMP4-induced ventral mesoderm patterning in differentiating ES cells. Development 2005;132:873–884.

32 Saga Y, Kitajima S, Miyagawa-Tomita S. Mesp1 expression is the earliest sign of cardiovascular development. Trends Cardiovasc Med 2000;10:345–352.

33 Bondue A, Lapouge G, Paulissen C et al. Mesp1 acts as a master regulator of multipotent cardiovascular progenitor specification. Cell Stem Cell 2008;3:69–84.

34 Buckingham M, Meilhac S, Zaffran S. Building the mammalian heart from two sources of myocardial cells. Nat Rev Genet 2005;6:826–835.

35 Moretti A, Caron L, Nakano A et al. Multipotent embryonic isl1+ progenitor cells lead to cardiac, smooth muscle, and endothelial cell diversification. Cell 2006;127:1151–1165.

36 Chen B, Dodge ME, Tang W et al. Small molecule-mediated disruption of Wnt-dependent signaling in tissue regeneration and cancer. Nat Chem Biol 2009;5:100–107.

37 O'Brien TX, Lee KJ, Chien KR. Positional specification of ventricular myosin light chain 2 expression in the primitive murine heart tube. Proc Natl Acad Sci USA 1993;90:5157–5161.

38 Bruneau BG, Bao ZZ, Tanaka M et al. Cardiac expression of the ventricle-specific homeobox gene Irx4 is modulated by Nkx2-5 and dHand. Dev Biol 2000;217:266–277.

39 Bao ZZ, Bruneau BG, Seidman JG et al. Regulation of chamber-specific gene expression in the developing heart by Irx4. Science 1999; 283:1161–1164.

40 Glinka A, Wu W, Delius H et al. Dickkopf-1 is a member of a new family of secreted proteins and functions in head induction. Nature 1998; 391:357–362.

41 Glukhova MA, Frid MG, Koteliansky VE. Developmental changes in expression of contractile and cytoskeletal proteins in human aortic smooth muscle. J Biol Chem 1990;265:13042–13046.

42 Bers DM. Cardiac excitation-contraction coupling. Nature 2002;415:198–205.

43 Feldman DS, Carnes CA, Abraham WT et al. Mechanisms of disease: Beta-adrenergic receptors—alterations in signal transduction

and pharmacogenomics in heart failure. Nat Clin Pract Cardiovasc Med 2005;2:475–483.

44 Ueno S, Weidinger G, Osugi T et al. Biphasic role for Wnt/beta-catenin signaling in cardiac specification in zebrafish and embryonic stem cells. Proc Natl Acad Sci USA 2007;104: 9685–9690.

45 Naito AT, Shiojima I, Akazawa H et al. Developmental stage-specific biphasic roles of Wnt/beta-catenin signaling in cardiomyogenesis and hematopoiesis. Proc Natl Acad Sci USA 2006;103:19812–19817.

46 Gessert S, Kühl M. The multiple phases and faces of wnt signaling during cardiac differentiation and development. Circ Res 2010;107:186–199.

47 Ni TT, Rellinger EJ, Mukherjee A et al. Discovering small molecules that promote cardiomyocyte generation by modulating Wnt signaling. Chem Biol 2011;18:1658–1668.

See www.StemCellsTM.com for supporting information available online.